Simulations of oscillatory convection in ^{3}He–^{4}He mixtures in moderate aspect ratio containers

Oriol Batiste[a] and Edgar Knobloch[b]
Department of Applied Mathematics, University of Leeds, Leeds LS2 9JT, United Kingdom

(Received 9 May 2004; accepted 28 March 2005; published online 26 May 2005)

Simulations of ^{3}He–^{4}He mixtures with negative separation ratios in two-dimensional containers with realistic boundary conditions and moderately large aspect ratio Γ are described. The system exhibits a large variety of states with complex time dependence including intermittent wave localization and chaotic "repeated transients." Steady but localized states are also found. Particular attention is paid to the transitions that occur for $(R-R_c)/R_c \approx \Gamma^{-2}$, where R is the Rayleigh number and R_c its critical value for the primary instability, in order to clarify the gradual transition from a small number of active degrees of freedom $[(R-R_c)/R_c \ll \Gamma^{-2}]$ to many active degrees of freedom $[(R-R_c)/R_c \gg \Gamma^{-2}]$. © *2005 American Institute of Physics*. [DOI: 10.1063/1.1920349]

I. INTRODUCTION

Binary fluid mixtures with a negative separation ratio exhibit a wide variety of behavior when heated from below. Of particular interest are the traveling-wave states with complex time dependence present very close to the onset of the primary instability.[1–4] In rectangular containers these include the so-called *blinking states*[2,3] and the *repeated transients*.[4] In such containers translation invariance is absent, and the eigenmodes of the linear stability problem are either odd or even under left-right reflection.[5] Recent work[6–8] shows that a description of the observed dynamics based on amplitude equations for such modes succeeds in capturing the behavior observed in both experiments and numerical simulations remarkably well.

Although the original experiments on overstable convection driven by the Soret effect were performed in salt-water mixtures,[9] subsequent experiments focused on ^{3}He–^{4}He (Refs. 1 and 10–12) and water-ethanol mixtures.[2–4] Of these the latter readily permit flow visualization, a fact invaluable for the interpretation of all measurements. However, the recent development of visualization techniques at cryogenic temperatures[13] offers the possibility that comparable experiments can now be performed on ^{3}He–^{4}He mixtures.

Detailed simulations of two-dimensional binary fluid convection in rectangular containers[8] are restricted to a water-ethanol mixture with separation ratio $S=-0.021$ in containers of aspect ratio $16 \leqslant \Gamma \leqslant 17$ and $|\epsilon| \equiv |R-R_c|/R_c \sim 10^{-3}$ or less, i.e., $|\epsilon| \ll \Gamma^{-2}$. Here R is the Rayleigh number and R_c is its critical value for the onset of overstability. The simulations employ experimental parameter values and boundary conditions, and reproduce much of the behavior reported in experiments.[4] In particular, they demonstrate the following:

- The experiments can be understood on the basis of two-dimensional simulations.
- In the regime $|\epsilon| \ll \Gamma^{-2}$ the behavior exhibited by the partial differential equations (and hence the experiments) is fundamentally low dimensional even though the aspect ratio Γ may be quite large.
- The primary instability takes the form of a subcritical bifurcation to an unstable time-periodic *chevron* state, consisting of traveling waves that propagate in opposite directions, usually outward from the center, in the two halves of the container. Such states are either odd or even under left-right reflection, and may acquire stability at finite amplitude via a saddle-node bifurcation.
- Stable blinking states are two-frequency states and set in when stable chevrons lose stability at a secondary Hopf bifurcation. The blinking amplitude increases with ϵ, and the blinking may become nonperiodic.
- In cases where the secondary Hopf bifurcation occurs on the unstable chevron branch below the saddle-node bifurcation the first observed state is the repeated transient state. This state is a three-frequency state, and may set in without observable hysteresis at $R=R_c$.
- With increasing ϵ the lowest frequency in the repeated transient state increases but its contribution decreases, and may disappear at a (typically hysteretic) Hopf bifurcation, leaving a large amplitude blinking state.
- Regular blinking states are observed near onset only for aspect ratios differing roughly by $\pi/k_c \approx 1$, corresponding to mode interaction points. Here k_c is the linear theory wave number.

Reference 8 did not, however, examine how the above results depend on the separation ratio $S<0$ of the mixture, or what happens as ϵ increases through the important regime $\epsilon \sim \Gamma^{-2}$, where additional spatial degrees of freedom become dynamically important. In particular, the details of the transition from oscillatory to steady states with increasing ϵ remain to be elucidated. We expect these to depend strongly on both S and Γ. To shed light on these questions and at the same time make specific predictions for a new physical sys-

[a]Also at Departament de Física Aplicada, Universitat Politècnica de Catalunya, Barcelona, Spain.
[b]Also at Department of Physics, University of California, Berkeley, CA 94720, USA.

tem we choose parameter values corresponding to ^{3}He–^{4}He mixtures, focusing on aspect ratio $\Gamma=10$. This choice reduces the extremely long transients that plagued the water-ethanol simulations, and permits us to investigate in considerable detail the sequence of transitions with increasing ϵ for different values of S. We show that a dramatic change in the behavior of the system occurs when oscillations persist into the regime $\epsilon \gtrsim \Gamma^{-2}$; in this regime front-like structures can localize the oscillations, leading to new types of oscillatory states and hence new mechanisms for the disappearance of time dependence. For small $|S|$ the oscillations exist in only a narrow interval of ϵ and remain spatially extended; we demonstrate that such oscillations disappear via a global bifurcation. For larger values of $|S|$ the small amplitude repeated transients and blinking states give rise to various types of traveling-wave pulses, typically localized in space and time. The transition to this state occurs via a state that we identify with the "fish state" observed in experiments on water-ethanol mixtures. Of particular interest is the observation of a novel state of spatially localized *steady* convection we call a "convecton." Some of our results are reported elsewhere.[14]

This paper is organized as follows. In Sec. II we summarize the basic equations, followed in Sec. III by the results of our numerical simulations. Section IV offers a theoretical insight into the regime $\epsilon \ll \Gamma^{-2}$ and, in particular, the origin of *chaotic* repeated transients. The paper concludes with a brief discussion.

II. THE GOVERNING EQUATIONS

Binary fluid mixtures are characterized by the presence of cross-diffusion terms in the diffusion matrix. In liquids the dominant cross-diffusion term is the Soret term, and the sign of this term determines the behavior of the mixture in response to an applied temperature gradient. For mixtures with a negative Soret coefficient the heavier component migrates towards the lower (hotter) boundary, i.e., a concentration gradient is set up that opposes the destabilizing temperature gradient that produced it. Under these conditions the onset of convection may take the form of growing oscillations. This instability, sometimes referred to as "overstability," may lead to a variety of states with complex time dependence in the nonlinear regime, as described elsewhere.[15] Here we focus on the corresponding behavior in ^{3}He–^{4}He mixtures. These differ from the water-ethanol mixtures studied elsewhere[8] primarily in having a substantially smaller Prandtl number.

We consider a binary mixture in a two-dimensional rectangular container $D \equiv \{x,z \,|\, 0 \leqslant x \leqslant \Gamma, -\frac{1}{2} \leqslant z \leqslant \frac{1}{2}\}$ heated uniformly from below, and nondimensionalize the equations using the depth of the layer as the unit of length and t_d, the thermal diffusion time in the vertical, as the unit of time. In the Boussinesq approximation appropriate to the experiments the resulting equations take the form[16]

$$\mathbf{u}_t + (\mathbf{u}\cdot\nabla)\mathbf{u} = -\nabla P + \sigma R[\theta(1+S) - S\eta]\hat{\mathbf{z}} + \sigma\nabla^2\mathbf{u}, \tag{1}$$

$$\theta_t + (\mathbf{u}\cdot\nabla)\theta = w + \nabla^2\theta, \tag{2}$$

$$\eta_t + (\mathbf{u}\cdot\nabla)\eta = \tau\nabla^2\eta + \nabla^2\theta, \tag{3}$$

together with the incompressibility condition

$$\nabla\cdot\mathbf{u} = 0. \tag{4}$$

Here $\mathbf{u} \equiv (u,w)$ is the velocity field in (x,z) coordinates, P is the pressure, and θ denotes the departure of the temperature from its conduction profile, in units of the imposed temperature difference ΔT. The variable η is defined such that its gradient represents the dimensionless mass flux. Thus $\eta \equiv \theta - C$, where C denotes the concentration of the heavier component relative to its conduction profile in units of the concentration difference that develops across the layer as a result of the Soret effect. The system is specified by four dimensionless parameters: the Rayleigh number R providing a dimensionless measure of the imposed temperature difference ΔT, the separation ratio S that measures the resulting concentration contribution to the buoyancy force due to the Soret effect, and the Prandtl and Lewis numbers, σ and τ, in addition to the aspect ratio Γ.

To model the experiments we take the boundaries to be no-slip everywhere, with the temperature fixed at the top and bottom and no sideways heat flux. The final set of boundary conditions is provided by the requirement that there is no mass flux through any of the boundaries. The boundary conditions are thus

$$\mathbf{u} = \mathbf{n}\cdot\nabla\,\eta = 0 \quad \text{on } \partial D, \tag{5}$$

and

$$\theta = 0 \quad \text{at } z = \pm 1/2, \quad \theta_x = 0 \quad \text{at } x = 0,\Gamma. \tag{6}$$

Here ∂D denotes the boundary of D.

Equations (1)–(6) are equivariant with respect to the operations

$$R_x: \quad (x,z) \to (\Gamma - x, z), \quad (\psi,\theta,C) \to (-\psi,\theta,C), \tag{7}$$

$$\kappa: \quad (x,z) \to (x,-z), \quad (\psi,\theta,C) \to (-\psi,-\theta,-C), \tag{8}$$

where $\psi(x,z,t)$ is the streamfunction, defined by $(u,w) = (-\psi_z, \psi_x)$. These two operations generate the symmetry group D_2 of a rectangle. It follows that even solutions, i.e., solutions invariant under R_x, satisfy $[\psi(x,z),\theta(x,z),C(x,z)] = [-\psi(\Gamma-x,z),\theta(\Gamma-x,z),C(\Gamma-x,z)]$ at each instant in time, while odd solutions are invariant under κR_x and satisfy $[\psi(x,z),\theta(x,z),C(x,z)] = [\psi(\Gamma-x,-z), -\theta(\Gamma-x,-z), -C(\Gamma-x,-z)]$, again at each instant of time. At midlevel, $z=0$, the latter therefore satisfy $[\psi(x,0),\theta(x,0),C(x,0)] = [\psi(\Gamma-x,0),-\theta(\Gamma-x,0),-C(\Gamma-x,0)]$, and so are odd in the conventional sense. It follows that the eigenfunctions of the conduction state $\psi=\theta=C=0$ are also even or odd; these, and the corresponding values of the critical Rayleigh number and frequency, are computed elsewhere[7] as a function of the aspect ratio Γ for $\sigma=0.6$ and $\tau=0.03$, and various values of the separation ratio S appropriate for ^{3}He–^{4}He experiments.[1] In the following we refer to the pure parity states as chevron states since they consist of waves traveling outwards from the center of the cell.

We solve Eqs. (1)–(6) in two dimensions using a time-splitting method with an improved boundary condition for

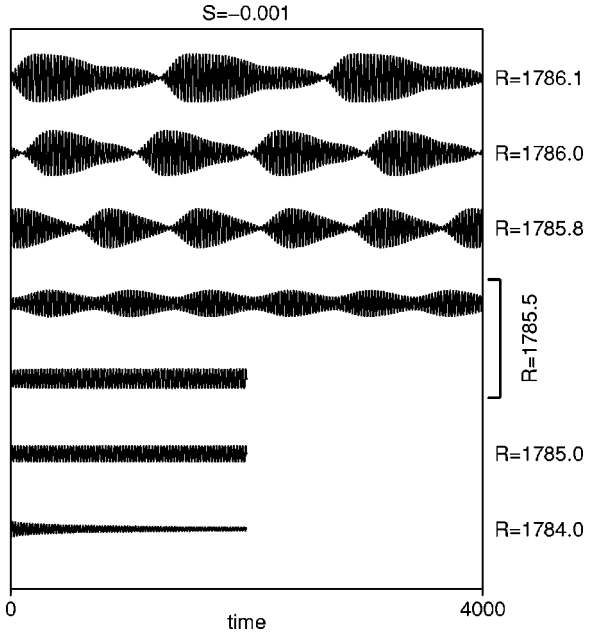

FIG. 1. Time series $w(x=0.87\Gamma,z=0,t)$ in a ^{3}He–^{4}He mixture with $S=-0.001$, $\sigma=0.6$, and $\tau=0.03$ for several different values of the Rayleigh number.

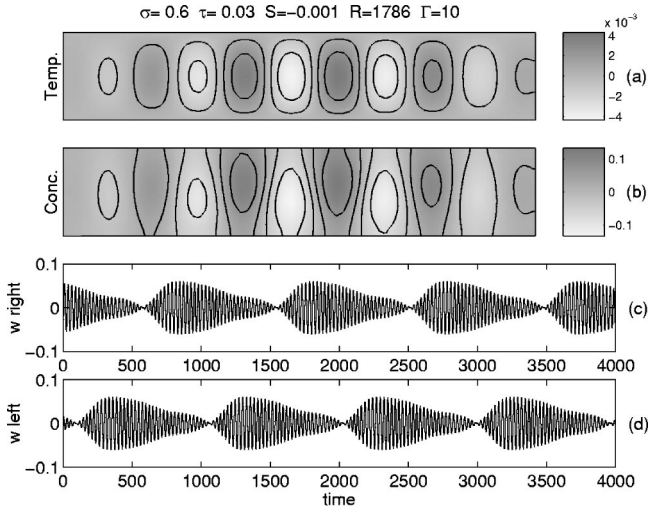

FIG. 2. As for Fig. 1 but showing a symmetric periodic blinking state at $R=1786$ ($\epsilon=1.1\times10^{-3}$). (a,b) Contours of $\theta(x,z,t)$ and $C(x,z,t)$ at $t=4000$. (c,d) $w(x=0.87\Gamma,z=0,t)$ and $w(x=0.13\Gamma,z=0,t)$.

the pressure and a second-order accurate time integration scheme based on a modified Adams–Bashforth formula.[17] For the spatial discretization we use a Chebyshev collocation pseudospectral method.[18] In all cases the time step and the number of collocation points used were adjusted until the solutions converged. Typically we used 170 collocation points in the x direction and 30 collocation points in the z direction, with a time step of $10^{-3}t_d$. We use the vertical velocity at the points $(x,z)=(0.13\Gamma,0)$ (near the left sidewall) and $(0.87\Gamma,0)$ (near the right sidewall) as a proxy for shadowgraph intensity measurements. Moreover, monitoring point quantities at mirror locations suffices to determine the spatial symmetry properties of the various possible time-dependent states. All our results use $\sigma=0.06$, $\tau=0.03$, and $\Gamma=10$. Four values of the separation ratio S are discussed in detail. In each case we describe the results of our simulations for increasing values of the reduced Rayleigh number $|\epsilon|$, and explore the transition from low-dimensional to high-dimensional behavior.

III. RESULTS

A. $S=-0.001$: Global bifurcation of blinking states

For $S=-0.001$ simulations of the growing instability at $R=1785>R_c\approx1784.088$ show that it saturates in an even-parity standing wave with frequency $\omega_1\approx0.25$, near the critical frequency $\omega_c\approx0.2675$. Figure 1 shows the time series of the saturated vertical velocity $w(x=0.87\Gamma,z=0,t)$, and indicates that the primary bifurcation is a supercritical Hopf bifurcation; no evidence of hysteresis was found. This result is consistent with available theory.[16] With increasing Rayleigh number this state undergoes a (slightly subcritical) Hopf bifurcation that introduces a new frequency ω_2 into the dynamics. The solution branch that results is initially unstable but acquires stability almost immediately at a saddle-node bifurcation. Figure 1 shows that stable single-frequency and two-frequency states coexist at $R=1785.5$. Strictly speaking this secondary Hopf bifurcation is a torus bifurcation. However, in the following we do not distinguish between Hopf bifurcations of equilibria and of periodic orbits (or tori), since resonance phenomena appear to play little role in the observed dynamics.

The two-frequency state can be identified with the blinking states predicted by abstract theory.[5,19,20] Figures 2(c) and 2(d) show that this state has the required symmetry; if we ignore for the moment the fast frequency ω_1 the blinking state has the spatiotemporal symmetry $R_x w(x,0,t)=w(x,0,t+T_2/2)$, where $T_2\equiv2\pi/\omega_2$ is the blinking period. In the following we refer to states of this type as *symmetric periodic blinking states*. When R is increased to $R=1786.2$ this state loses stability and the system jumps to a large amplitude even-parity steady state (Fig. 3). The modulation period T_2 appears to diverge logarithmically as this transition is approached (Fig. 4), suggesting that the oscillations disappear when the two-torus collides with an (unstable) steady-state branch. A fit to the theoretical prediction

$$T_2=-2\lambda_u^{-1}\ln|R-R_h|+d \tag{9}$$

leads to the estimates $R_h\approx1786.112$, $\lambda_u\approx0.2452$, and d

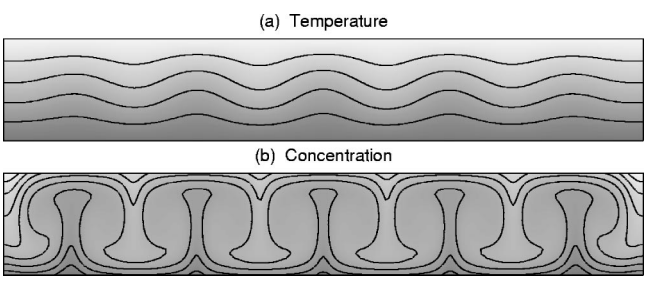

FIG. 3. The large amplitude steady state reached when R is increased from $R=1786$ to $R=1786.2$ when $S=-0.001$, $\sigma=0.6$, and $\tau=0.03$.

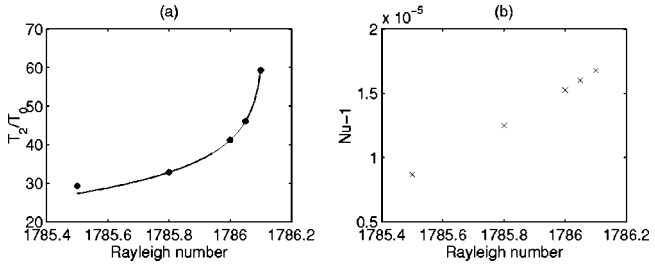

FIG. 4. (a) The blinking period T_2 in units of the Hopf period $T_o \equiv 2\pi/\omega_c$ as a function of R near the transition to steady convection when $S=-0.001$, $\sigma=0.6$, and $\tau=0.03$. The solid line represents the fit (9). (b) The corresponding Nusselt number.

≈ 8.1537. Here λ_u is to be identified with the leading *unstable* eigenvalue of the steady state at $R=R_h$.

B. $S=-0.021$: The fish state

Figure 5 shows that when $S=-0.021$ the transition to steady convection is quite different. Although the primary instability is still to an even mode ($R_c=1855.75$ and $\omega_c=2.076$) the bifurcation is now slightly hysteretic, so that stable even chevrons are present even for $R<R_c$ (not shown). As R is raised a second frequency appears in the time series, corresponding to the onset of a symmetric blinking state. This bifurcation is apparently also subcritical, but once again the resulting blinking states acquire stability in a saddle-node bifurcation. This behavior is qualitatively similar to that described for $S=-0.001$. However, with increasing

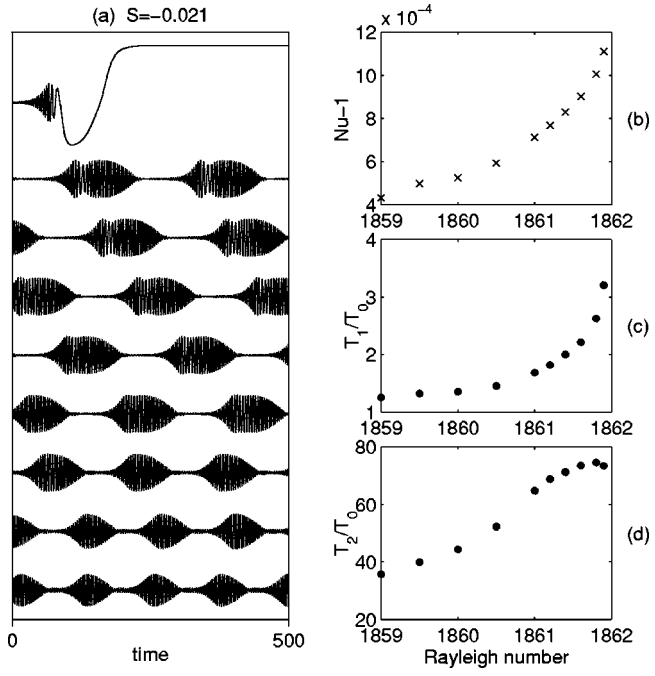

FIG. 5. A ^{3}He–^{4}He mixture with $S=-0.021$, $\sigma=0.6$, and $\tau=0.03$ in a $\Gamma=10$ container. (a) Time series $w(x=0.87\Gamma, z=0, t)$ for different values of R increasing upwards ($1859.5<R<1862.0$), showing a hysteretic transition to steady convection at $R\approx 1862.0$ ($\epsilon=3.4\times10^{-3}$). (b) The corresponding Nusselt number as a function of R. (c) The chevron period $T_1\equiv 2\pi/\omega_1$ as a function of R. (d) The blinking period $T_2\equiv 2\pi/\omega_2$ as a function of R. The state at $R=1861.8$ resembles the *fish state* observed in the experiments.

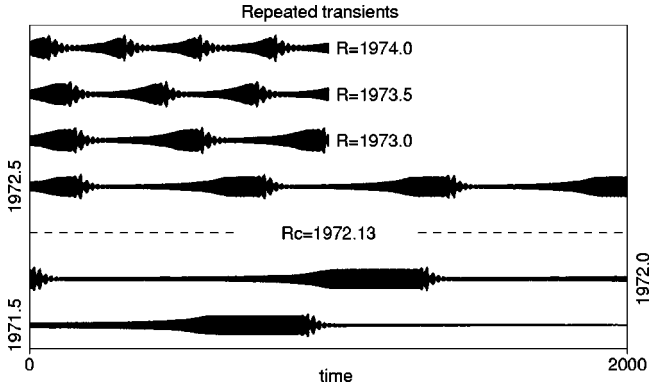

FIG. 6. The repeated transient state in a ^{3}He–^{4}He mixture with $S=-0.1$, $\sigma=0.6$, $\tau=0.03$, and $\Gamma=10$ at several values of R. The time series $w(x=0.87\Gamma, z=0, t)$ suggest the presence of three frequencies, with the lowest-frequency ω_3 increasing from zero as R increases from $R\approx 1971.5$ ($\epsilon=\epsilon^*\approx -3.2\times10^{-4}$).

R the modulation period T_2 begins to increase but then apparently saturates at a finite value [Fig. 5(d)]. At the same time the period $T_1\equiv 2\pi/\omega_1$ appears to diverge [Fig. 5(c)]. These properties are reflected in the time series presented in Fig. 5(a), which show that at $R=1862.0$ the blinking state loses stability to steady convection from the lowest-frequency portion of the wavetrain, and indicate that the transition to steady convection now occurs via a radically different mechanism (see below). In the following we refer to the state just prior to this transition as the *fish state*. Similar states have been observed in water-ethanol mixtures.[2]

C. $S=-0.1$: From repeated transients to the fish state

The case $S=-0.1$ is even more interesting. Here $R_c=1972.13$ and $\omega_c=4.918$. In this case the primary bifurcation to the (even) chevron state is substantially subcritical,[16] and the first stable nonlinear state takes the form of a repeated transient (Fig. 6). States of this type were studied in detail by Kolodner in experiments on water-ethanol mixtures,[4] and their origin is discussed in Ref. 8. Figure 6 suggests (and the theory of Sec. IV confirms) that these states are *three-frequency* states, in which ω_1 is the fast chevron frequency, ω_2 represents the blinking frequency, while the third frequency ω_3 represents the slow modulation frequency. Detailed study shows that the repeated transient consists of a slowly growing (even) chevron state that eventually becomes unstable to the onset of blinking, which leads to a collapse of the state back to a small amplitude (even) chevron, followed by a slow regrowth. In the time series shown these collapse events are periodic with period $T_3=2\pi/\omega_3$. Figure 7 shows that as R decreases the period $T_3=2\pi/\omega_3$ increases rapidly and apparently diverges at $R\approx 1971.5$. Such a divergence suggests that the three-frequency states are created via a global bifurcation. Since no stable nonzero solutions are present for smaller values of R for these parameter values the three-frequency repeated transient state represents the *first* nontrivial state of the system, much as occurs in water-ethanol mixtures.[4,8] This interesting property of the system is explained in Sec. IV.

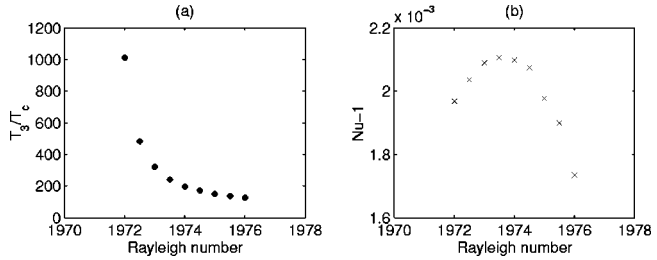

FIG. 7. (a) The modulation period $T_3 \equiv 2\pi/\omega_3$ of the repeated transients when $S=-0.1$, $\sigma=0.6$, $\tau=0.03$, and $\Gamma=10$ in units of $T_o \equiv 2\pi/\omega_c$ as a function of the Rayleigh number R. (b) The corresponding Nusselt number.

In contrast, as R increases the modulation frequency ω_3 increases but drops out from the time series between $R=1980.0$ and $R=1981.0$ (Fig. 8). We identify this transition with a Hopf bifurcation,[8] and note that Fig. 8 indicates that this bifurcation is *supercritical*, i.e., viewed in the direction of decreasing R this bifurcation creates a *stable* three-frequency state from a stable two-frequency state, with no observable hysteresis. Figure 9 shows that this two-frequency state is a symmetric blinking state, and traces the evolution of this state towards larger values of R. The figure shows that at $R=1995$ the blinking has become asymmetric and nonperiodic, while the time series for $R=2000$ and $R=2005$ may be periodic, but are strongly asymmetric. In contrast, when $R=2010$ the blinking becomes once again periodic and symmetric. None of these transitions appears to be hysteretic. At yet larger values of R these states again evolve into the fish state, followed by a transition to stationary convection. Figure 10 shows an example of the fish state just prior to this transition. An examination of the spatial structure of the waves (Fig. 11) shows that there is a brief phase of the oscillation during which small amplitude counter-propagating waves fill the container. This state is highly unstable, however, with the waves at one end growing at the expense of those at the other. Once the amplitude of the growing state is large enough the system shifts into a new and larger amplitude state in which the waves are spatially confined towards one side, with *no* waves at the other [see Figs. 11 and 12(a)]. This transition is marked by a dramatic drop in the frequency ω_1 since the waves in this pulse-like state travel much more slowly. We surmise that this is due to the large amplitude of this state. This change in frequency in turn increases the Nusselt number, and does so despite the fact that the waves no longer fill the whole domain. As time proceeds this confined state drifts in the direction of the waves within it, and settles next to the boundary, forming a wall-attached state [see Figs. 11 and 12(b)]. During the attachment process the localized state contracts and its amplitude decreases, presumably due to increased dissipation. As a

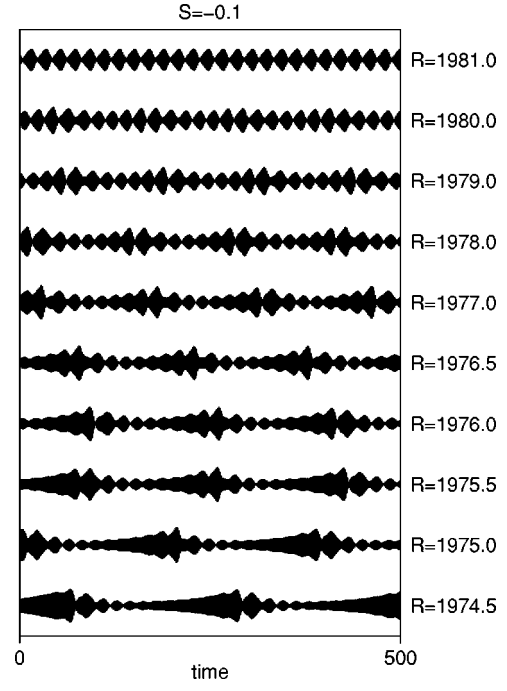

FIG. 8. The time series $w(x=0.87\Gamma, z=0, t)$ for a ^{3}He$-^4$He mixture with $S=-0.1$, $\sigma=0.6$, $\tau=0.03$, and $\Gamma=10$ at several values of R showing the transition from the repeated transient state in Fig. 6 to a symmetric periodic blinking state at $R=1981$ ($\epsilon=4.5\times10^{-3}$).

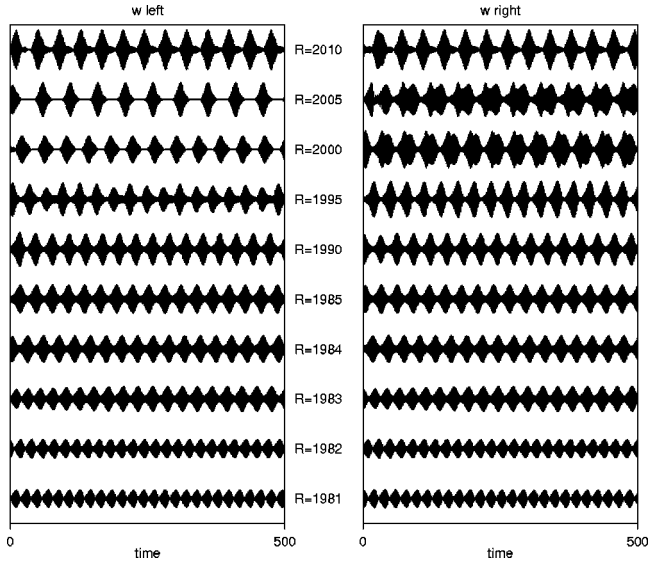

FIG. 9. Time series $w(x=0.13\Gamma, z=0, t)$ (left column) and $w(x=0.87\Gamma, z=0, t)$ (right column) for different values of R increasing upwards, and $S=-0.1$, $\sigma=0.6$, $\tau=0.03$, and $\Gamma=10$.

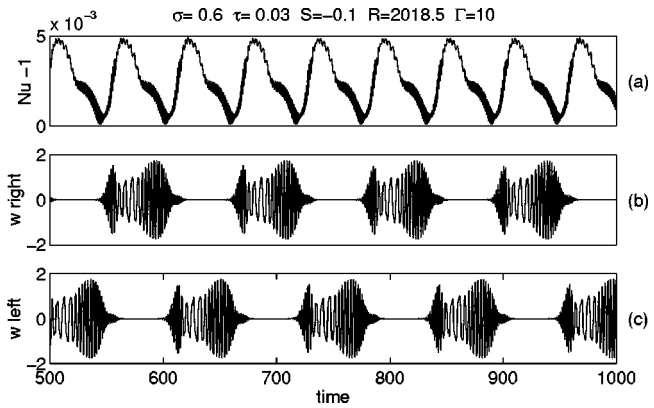

FIG. 10. (a) The Nusselt number $\mathrm{Nu}(t)$, (b) $w(x=0.87\Gamma, z=0, t)$, (c) $w(x=0.13\Gamma, z=0, t)$ for $R=2018.5$ ($\epsilon=0.024$), and $S=-0.1$, $\sigma=0.6$, $\tau=0.03$, and $\Gamma=10$.

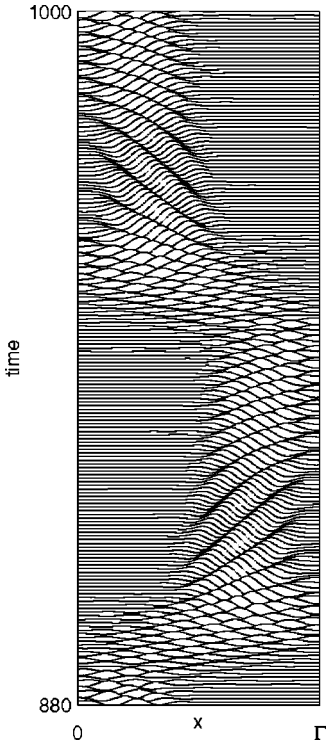

FIG. 11. Space-time plot of the fish state in Fig. 10 with time increasing upwards. The state is periodic in time with period T, and is invariant under the spatial reflection R_x followed by evolution for a time $T/2$.

result ω_1 increases again. During this process $w(x=0.87\Gamma, z=0, t)$ actually increases as activity moves to the region where w is measured. However, integral quantities such as the Nusselt number actually decrease, since the amplitude of the state falls on contact with the wall. The appearance of the prominent shoulder in the Nusselt number time series [Fig. 10(a)] coincides with the formation of the wall-attached state. The wall-attached state is not stable, however, and continues to decrease in amplitude and contract until it becomes so weak and confined that waves start to regrow at the other sidewall. At this point the wall-attached state disintegrates, and the small amplitude extended chevron-like state is restored. All these transitions are quite easily distinguished in the time trace shown in Fig. 10 and in the space-time plot shown in Fig. 11, and suggest that the formation of the initial pulse-like state is triggered by a nonlinear focusing effect reminiscent of the nonlinear Schrödinger equation.

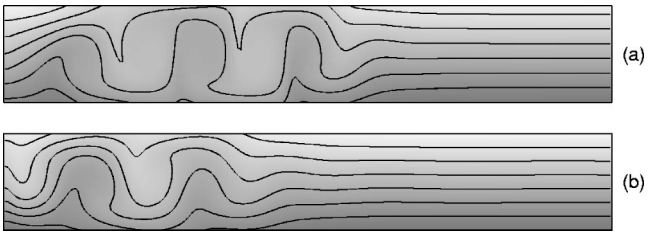

FIG. 12. Concentration contours during (a) the low-frequency part of the fish state in Fig. 10, and (b) during the high-frequency phase that follows it. The localized state in (a) settles against the left sidewall forming temporarily the wall-attached left-traveling wave shown in (b).

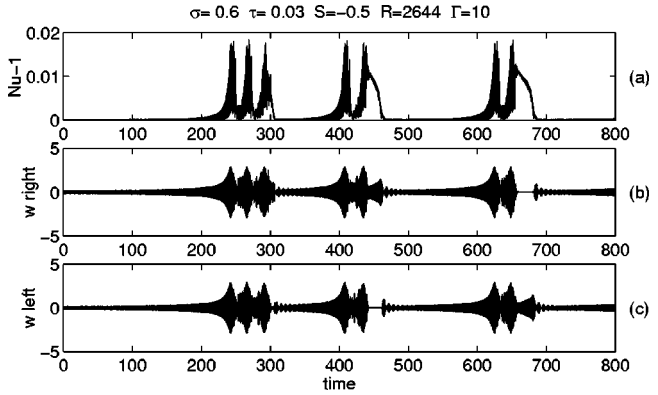

FIG. 13. (a) The Nusselt number Nu(t), (b) $w(x=0.87\Gamma, z=0, t)$, (c) $w(x=0.13\Gamma, z=0, t)$ for $R=2644$ ($\epsilon=2.1\times10^{-4}$), and $S=-0.5$, $\sigma=0.6$, $\tau=0.03$, and $\Gamma=10$, showing irregular bursts.

Many of the above details resemble behavior observed in experiments on water-ethanol mixtures[21] (see Fig. 1 of Ref. 21), although in some cases[22] the frequency ω_1 *drops* as the confined state settles near the lateral wall. It is possible that this is because in this experiment the pulse drifts in a direction *opposite* to the waves within it (anomalous nonlinear dispersion). Experiments suggest that this occurs when $\epsilon<0$,[23] while in our simulations $\epsilon>0$.

D. $S=-0.5$: Convective bursts, spatially localized traveling waves, and convectons

The final case we have considered is $S=-0.5$. Here $R_c=2643.43$ and $\omega_c=12.836$. The primary instability is again to an even chevron, but this time we find strongly irregular dynamics already quite close to onset (Fig. 13). The time series in Fig. 13 is best described as an intermittent repeated transient, in which the final collapse event may be preceded by several spatially symmetric bounces before the onset of the symmetry-breaking instability that disrupts the state and leads to the temporary formation of a confined state towards one side, much as already described for $S=-0.1$. This state then drifts towards the nearest wall and shrinks in lateral extent, until it triggers another collapse event that permits waves to grow at the other sidewall. The decaying symmetric blinking state that results reestablishes a small amplitude chevron state which then regrows on a much longer time–scale. The spatially symmetric bounces are associated with relatively sharp peaks in the Nusselt number, while the symmetry-breaking collapse events produce bursts in the Nusselt number that are markedly asymmetric, much as in the fish state discussed above.

The frequency of the burst-like events in the Nusselt number increases with R (Fig. 14). A periodic sequence of bursts, produced by a symmetric albeit complex state, is shown in Fig. 15. Perhaps the most remarkable time series of all is shown in Fig. 16 for $R=2750$ (see also the corresponding space-time diagram in Fig. 17). The time series apparently shows an irregular switching between two states, a large amplitude state with a relatively low ω_1, and a small amplitude state with a large ω_1. The former is a spatially confined slowly drifting wave, while the latter is an extended

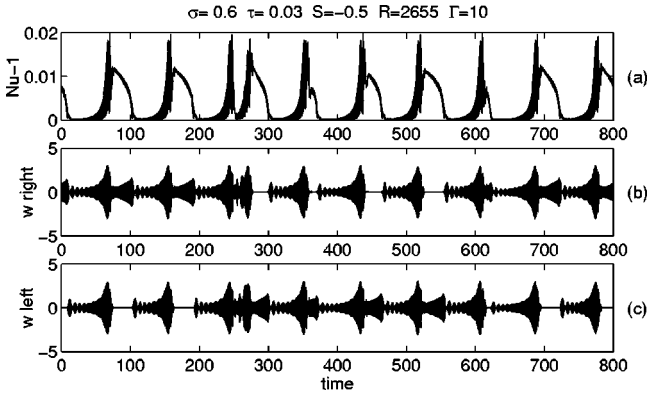

FIG. 14. As for Fig. 13 but showing the time series corresponding to $R=2655$ ($\epsilon=4.4\times10^{-3}$).

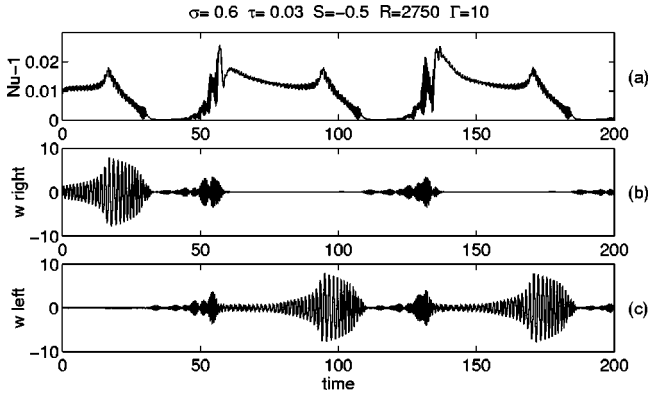

FIG. 16. Irregular switching between the fish state and a blinking state at $R=2750$ ($\epsilon=0.040$).

more-or-less symmetric pulsating chevron-like state. The latter is unstable to a symmetry-breaking blinking instability which amplifies the waves near one of the sidewalls at the expense of those near the opposite wall. The amplified waves are then reflected from the wall but continue to grow, slowing down markedly. This asymmetric state then abruptly collapses (by a mechanism that remains unclear) into a highly nonlinear spatially confined state consisting of slowly traveling waves. These waves propagate in the direction of the original reflected wave, and speed up as they approach the opposite wall. The whole pulse gradually retracts towards that wall, ultimately leaving much of the cell free of convection. Once the peak of the pulse reaches the wall its amplitude drops dramatically and it disintegrates into smaller amplitude counterpropagating waves that invade the convection-free part of the container, permitting the regrowth of the original higher-frequency small amplitude chevron-like state filling the domain (Fig. 17). Overall this behavior resembles that observed for $S=-0.1$ (see Figs. 11 and 12) but here it is much more dramatic, and we may think of it as back-and-forth "sloshing." The resulting state is reminiscent of a state found in doubly diffusive convection.[24,25]

In Fig. 18 we show a stable wall-attached traveling wave found at $R=2900$. A wave of this type evolves from the fish state when the localized low-frequency state comes to rest against a sidewall, but does not collapse. The resulting state should be interpreted in terms of a stationary *front* separating an exponentially small wave throughout most of the domain from a finite amplitude wavetrain next to the left sidewall. This interpretation of Fig. 18 is supported by the spectrum of the vertical velocity w near the left and right sidewalls [Fig. 18(c)]: both spectra have the *same* dominant frequency ω_1, with prominent harmonics near the left sidewall where the wave is localized, and much weaker harmonics near the right sidewall where it is exponentially small. Note, in particular, the absence of a right-traveling wave in any part of the container except perhaps right next to the *left* sidewall where a right-traveling component is required to set up a standing oscillation. Thus Fig. 18 represents a stable dynamically localized state, in contrast to both the kinematically localized

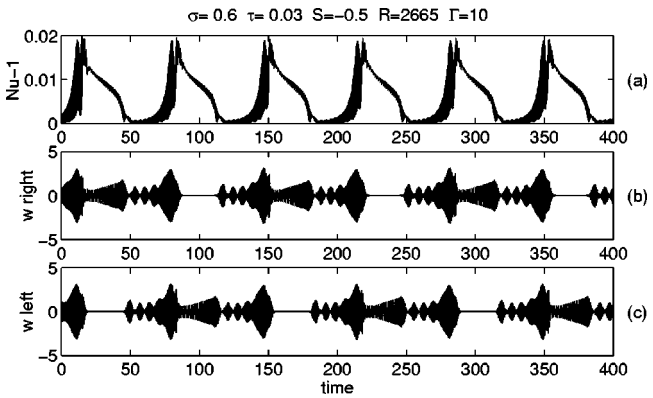

FIG. 15. As for Fig. 13 but showing periodic bursts at $R=2665$ ($\epsilon=8.2\times10^{-3}$).

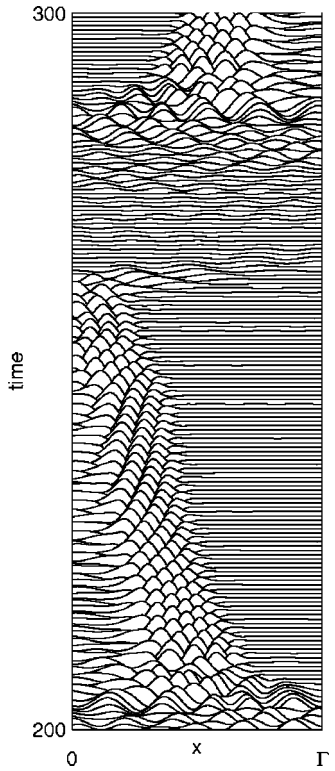

FIG. 17. Space-time plot of the state in Fig. 16 with time increasing upwards.

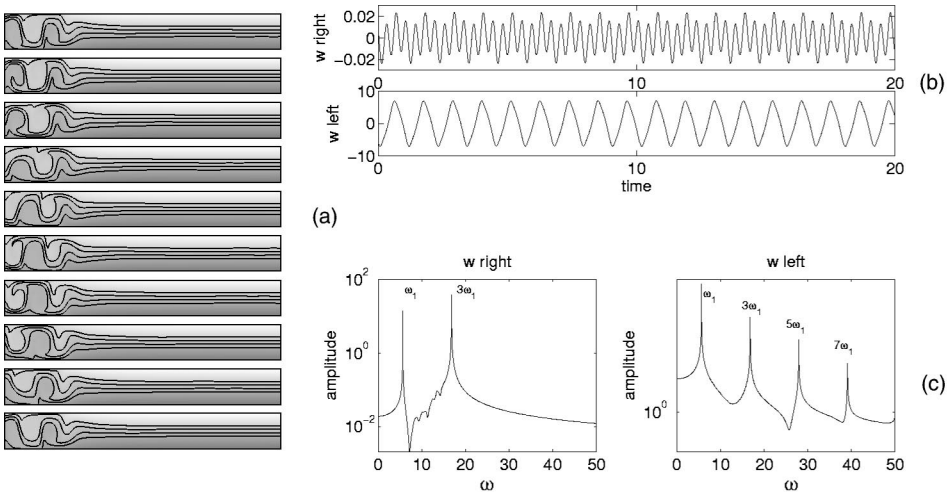

FIG. 18. (a) A left-traveling wave confined to the left sidewall when $R=2900$ ($\epsilon=0.097$), and $S=-0.5$, $\sigma=0.6$, $\tau=0.03$, and $\Gamma=10$, shown in terms of the total concentration contours, with time increasing upwards. (b) The corresponding vertical velocity $w(x=0.87\Gamma,z=0,t)$ and $w(x=0.13\Gamma,z=0,t)$, and (c) their Fourier transforms. The frequencies ω_1 in the two panels are identical. Note the different vertical scales in (b).

state present when $\epsilon \ll \Gamma^{-2}$, and the unstable dynamically localized waves that briefly form for smaller values of R (but satisfying $\epsilon \gtrsim \Gamma^{-2}$). Similar states have been observed in water-ethanol experiments[26–28] and related simulations.[29,30] States of this type are described well by a *single* complex Ginzburg–Landau equation with a drift, and become possible only once $|\epsilon| \gg \Gamma^{-2}$. Theory based on this equation predicts[31–33] that with increasing R the front gradually moves towards the right, but in the present case the strong nonlinear dispersion forces the frequency towards zero; once this occurs the resulting nonoscillatory state begins to expand towards the right by adding (steady) rolls and thereby expelling the lateral concentration gradient set up by the confined traveling wave. The process of adding rolls terminates once this lateral gradient is sufficiently strong, and results in the formation of a spatially confined but *steady* state (see Fig. 19). Such confined steady states have also been found for other values of R (Fig. 20), indicating that the confined states created by this process are in general non–unique. All of these states are numerically stable. Continuation methods indicate that these confined steady states retain their character with varying Rayleigh number, and lie on disconnected solution branches (cf. Fig. 21). In particular, the localized traveling wave in Fig. 18 is located on a *different* branch of solutions than the states shown in Figs. 19 and 20. Unfortunately, the origin of the confined steady states and their fate at larger Rayleigh numbers remain unknown. To our knowledge no comparable states have been observed in any experiment.

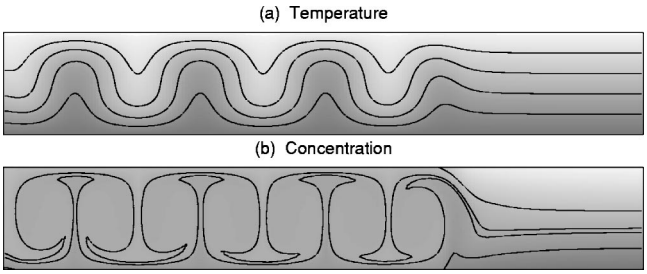

FIG. 19. A stable spatially confined steady state at $R=3050$ ($\epsilon=0.154$) when $S=-0.5$, $\sigma=0.6$, $\tau=0.03$, and $\Gamma=10$.

These confined steady states and their nonuniqueness are reminiscent of the slowly drifting pulses that form in binary fluid mixtures as a result of an interaction between the waves and a slowly evolving mean concentration mode;[34,35] near onset spontaneously developing inhomogeneities in the mean concentration field can trap pulses of traveling waves by decreasing the growth rate of the waves in front of the pulse, thereby braking its drift. However, in the absence of lateral boundaries the pulses always drift, albeit slowly, and only in exceptional cases is a stationary pulse possible. In systems with lateral boundaries such pulses come to rest at the lateral walls forming a wall-attached state, but in general the traveling waves within them will continue to propagate, much as in Fig. 18. In contrast, the localized steady states found here are present far from the onset of the primary oscillatory instability, and resemble instead the *convectons* present in strongly nonlinear magnetoconvection.[36] In our system these localized steady states are also confined by horizontal gradients in the concentration field [see Fig. 19(b)] stabilized by incident small amplitude traveling waves,[37] or a weak but steady large scale recirculation on either side. As a result the essence of the nonuniqueness is also different. In the theory[35] short and long pulses of a definite size can coexist stably; in our system the lateral boundaries may well support whatever

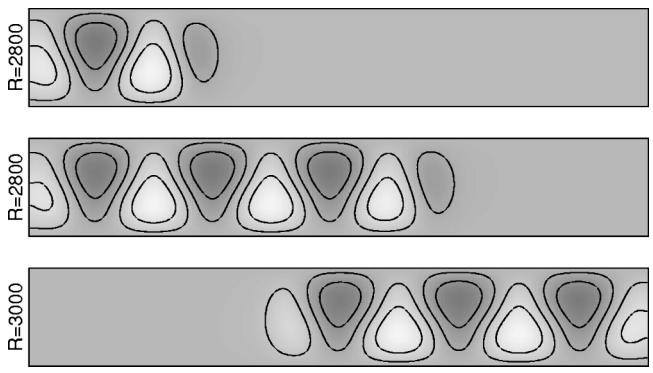

FIG. 20. Additional stable spatially confined steady states when $S=-0.5$, $\sigma=0.6$, $\tau=0.03$, and $\Gamma=10$, shown in terms of the contours of the fluctuating temperature $\theta(x,z)$. The corresponding value of R is indicated at the right of each panel.

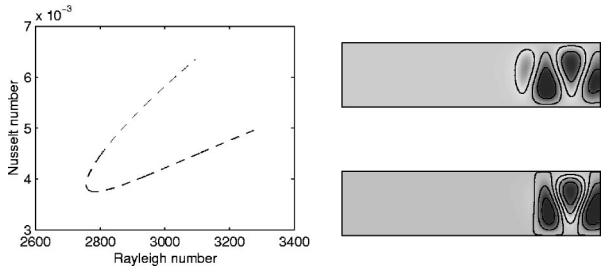

FIG. 21. The branch of confined steady states corresponding to the state shown in Fig. 20(a). The upper contour plot of $\theta(x,z)$ corresponds to the upper endpoint on the curve; the lower contour plot corresponds to the lower endpoint. The upper convecton is stable between the turning point and $R\approx 2800$; the lower is unstable.

concentration gradient is required to confine a particular state, suggesting that a large number of states, containing different numbers of roll pairs, may be stable simultaneously.

Figures 22 and 23 suggest that there is a wide variety of coexisting time-dependent states as well. The former shows a stable *odd*-parity chevron state with a superposed small amplitude temporal modulation that coexists with the state shown in Fig. 13 that is based on an even chevron. Figure 22 shows that the modulation is exactly out of phase in the two halves of the domain, and although it has a complex waveform it appears to be periodic in time. This state is therefore a symmetric blinking state, and indeed with decreasing R one finds that the modulation disappears and (at $R=2606$) a stable odd-parity chevron is recovered. Likewise, Fig. 23 shows a chaotic blinking state at $R=2665$ that is also based on an odd-parity chevron and coexists stably with the bursts shown in Fig. 15 that are based on an even chevron. This multistability greatly complicates the behavior of the system, and appears to be a consequence of increasing subcriticality of the primary bifurcations with decreasing separation ratio.[16]

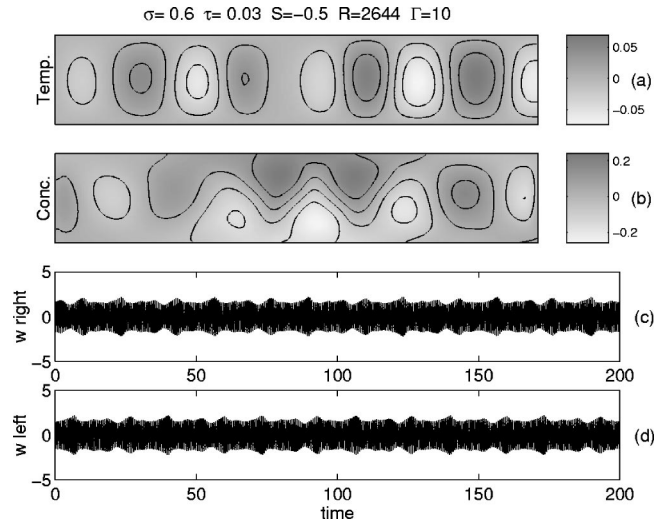

FIG. 22. Odd-parity chevron state with a superposed small amplitude temporal modulation for $R=2644$ ($\epsilon=2.1\times10^{-4}$). (a,b) Contours of $\theta(x,z,t)$ and $C(x,z,t)$ at $t=200$. (c,d) $w(x=0.87\Gamma,z=0,t)$ and $w(x=0.13\Gamma,z=0,t)$. This state coexists with the state in Fig. 13.

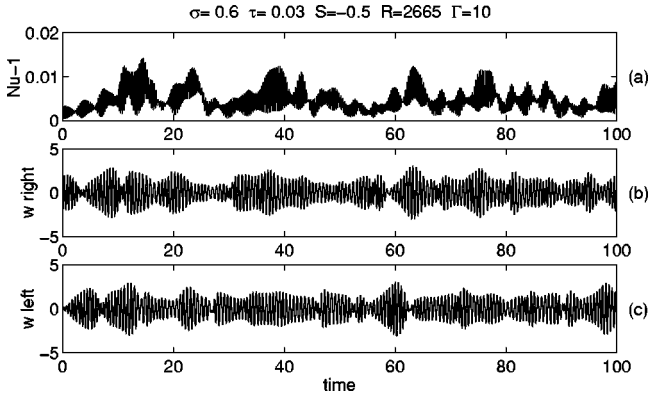

FIG. 23. A stable chaotic blinking state at $R=2665$ ($\epsilon=8.2\times10^{-3}$) based on an odd-parity chevron that coexists with the bursts shown in Fig. 15.

IV. ORIGIN OF THE BLINKING STATES AND REPEATED TRANSIENTS

In this section we summarize the properties of a simple model system, based on normal form theory for the interaction of two Hopf modes with opposite parity, that accounts for essentially all the properties revealed in our simulations when $\epsilon\ll\Gamma^{-2}$. We do not have a corresponding understanding of the dynamics observed at larger Rayleigh numbers. The model is based on the observation that, at specific aspect ratios Γ_c, the odd and even chevrons bifurcate simultaneously, albeit with different frequencies.[7] For nearby aspect ratios they come in, in close succession. Under these conditions we may expect the chevrons to interact in the nonlinear regime, and to do so already at small amplitude. We write each of the fields ψ, θ, and C in the form

$$\theta(x,z,t)=\mathrm{Re}\{z_+(t)e^{i\omega_+t}f_+(x,z)+z_-(t)e^{i\omega_-t}f_-(x,z)\}+\cdots, \tag{10}$$

where $f_\pm(x,z)$ are the (complex) eigenfunctions of the even and odd chevrons,[7] and $z_\pm(t)$ are their amplitudes. Standard normal form theory now yields the following equations for the (real) amplitudes $r_\pm\equiv|z_\pm|$:

$$\dot r_+=(\mu+a_+r_+^2+b_+r_-^2-r_+^4+c_+r_+^2r_-^2+d_+r_-^4)r_++\cdots, \tag{11}$$

$$\dot r_-=(\mu-\delta+a_-r_-^2+b_-r_+^2-r_-^4+c_-r_+^2r_-^2+d_-r_+^4)r_-+\cdots, \tag{12}$$

with a pair of decoupled equations for the associated (nonlinear) frequencies $\omega_\pm$. Here the coefficients are all real, and we take $a_\pm>0$ so that both chevrons bifurcate subcritically, the even ones [given by $(z_+,z_-)=(r_+,0)\exp i\omega_+t$] at $\mu=0$ and the odd ones [given by $(z_+,z_-)=(0,r_-)\exp i\omega_-t$] at $\mu=\delta>0$. It is now a simple matter to show that the two chevrons undergo saddle-node bifurcations at $\mu=-a_\pm^2/4<0$, and steady-state bifurcations to a mixed parity state (z_+,z_-), $r_+r_->0$, at $\mu=\delta-b_-r_+^2-d_-r_+^4$ (even chevrons) and $\mu=-b_+r_-^2-d_+r_-^4$ (odd chevrons). The bifurcations to the mixed parity states are to be identified with Hopf (more precisely torus) bifurcations from the chevron states to blinking states. This is because near this bifurcation on the even chevron branch the dynamics takes the form

$$\theta(x,z,t) = \mathrm{Re}\, r_+ e^{i\omega_+ t}\{f_+(x,z) + (r_-/r_+)e^{i(\omega_- - \omega_+)t} f_-(x,z)\} + \cdots, \tag{13}$$

describing an even chevron with a periodically oscillating odd-parity contribution. The second term amplifies (reduces) waves in the left half of the container at the same time as it reduces (amplifies) waves in the right half, and shows that the blinking frequency at leading order is simply the beat frequency $\omega_2 = \omega_+ - \omega_-$. We emphasize that these frequencies are the *nonlinear* frequencies, not the onset frequencies predicted by linear theory.

When this bifurcation occurs below the saddle-node bifurcation on the chevron branch the blinking states are initially unstable but acquire stability with increasing amplitude at a *tertiary* Hopf bifurcation.[38,39] This bifurcation introduces a *third* frequency ω_3 into the dynamics of the system; the resulting three-frequency states can be identified with the repeated transients.[8]

The key transitions involving the one-, two-, and three-frequency states are captured by a simplified model system obtained from the above equations by dropping inessential terms. In particular, we drop the term $-r_-^5$ and mimic its effect by taking $a_- < 0$. The resulting model[8]

$$\dot{r}_+ = (\mu + a_+ r_+^2 - r_+^4 - r_-^2) r_+, \tag{14}$$

$$\dot{r}_- = (-\nu + a_- r_-^2 + b_- r_+^2) r_-, \tag{15}$$

with $a_+ > 0$, $b_- > 0$, is the simplest set of equations capable of describing correctly the stability properties of the even chevrons and the mixed parity states observed in the partial differential equations for moderate values of $|S|$. The model removes the primary bifurcation to the odd chevrons but leaves the secondary bifurcations from the even chevrons fundamentally unchanged. In the following we think of μ and ν as proportional to $R - R_c(\Gamma)$ and $\Gamma - \Gamma_c(R)$, respectively.

Figure 24 summarizes the properties of the model in the case in which the three-frequency state created from the blinking state branch is stable. This is always the case when $b_- = 1$, $a_- = 0$, and $a_+ > 0$, and hence for sufficiently small negative values of a_- as well. The figure shows the loci of the primary (H_1), secondary (H_2), and tertiary (H_3) Hopf bifurcations, as well as the locus of the saddle-node (SN) bifurcations on the chevron branch. It should be remembered that in the (r_+, r_-) variables only the bifurcation H_3 remains a Hopf bifurcation, with H_1 and H_2 represented by pitchfork bifurcations. In addition the figure shows the curve $\gamma: \mu = \mu^*(\nu)$ of global bifurcations at which the limit cycle (corresponding to the three-frequency states) created at H_3 disappears by simultaneous collision with small and large amplitude chevron states. The location of this line must be determined numerically. An asymptotic calculation of this curve near the codimension-two point at which H_2 and SN coincide yields the heavy broken line; this line is tangent to γ at the codimension-two point, as it must.

Figure 25(a) shows the bifurcation diagram obtained by traversing the (μ, ν) plane in Fig. 24 along the line $\nu = 1.6$. The figure shows a small interval of subcritical but stable chevrons, followed by a supercritical pitchfork bifurcation to

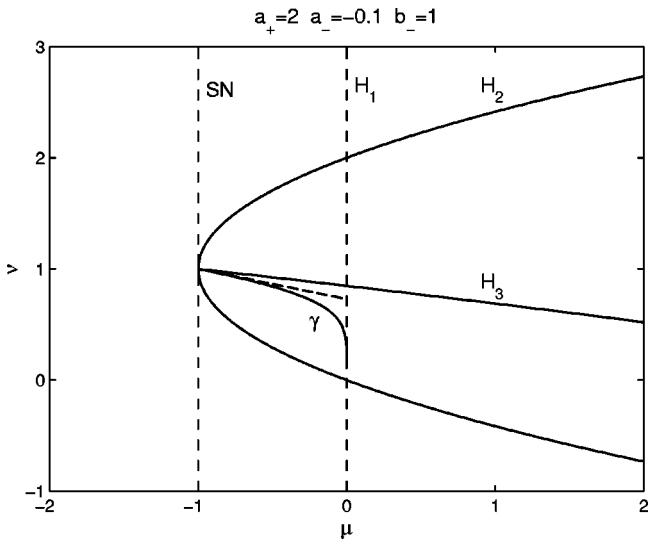

FIG. 24. Codimension-one bifurcation surfaces in the (μ, ν) plane for Eqs. (14) and (15) with $a_+ = 2.0$, $a_- = -0.1$, and $b_- = 1.0$. H_1: primary (Hopf) bifurcation to the chevron state $(r_+, 0)$, SN: saddle-node bifurcation on the chevron branch, H_2: (secondary) Hopf bifurcation to blinking states (r_+, r_-), H_3: (tertiary) Hopf bifurcation from (r_+, r_-) responsible for the appearance of the three-frequency states, and γ: global bifurcation at which these states disappear. The heavy broken line represents the asymptote to γ.

a state with $r_- \neq 0$ that represents a blinking state in the physical variables. In the example shown this bifurcation occurs at $\mu < 0$ so that the first stable state just above the onset ($\mu = 0$) is a finite amplitude blinking state. This case is typical of the behavior of the partial differential equations for $S = -0.01$ in appropriate ranges of Γ (not shown). The behavior shown in Fig. 1 for $S = -0.001$ is also of this type except

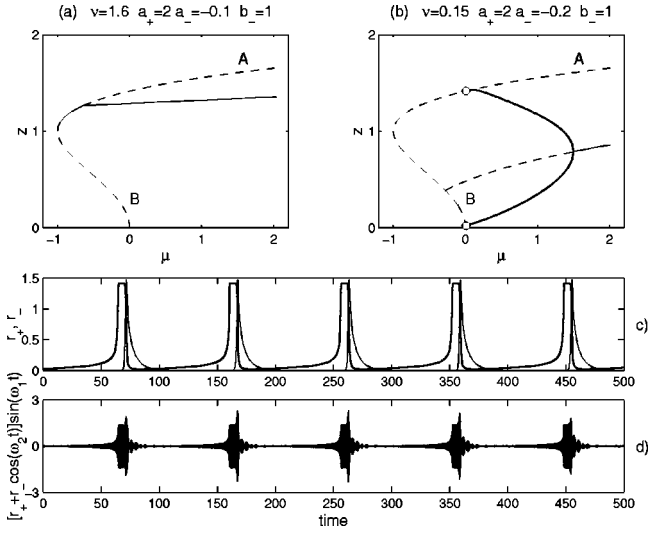

FIG. 25. Bifurcation diagrams along (a) the line $\nu = 1.6$ when $a_+ = 2.0$, $a_- = -0.1$, and $b_- = 1.0$, and (b) the line $\nu = 0.15$ when $a_+ = 2.0$, $a_- = -0.2$, and $b_- = 1.0$. The open circles indicate the global bifurcation; this bifurcation occurs very close to $\mu = 0$ for a large range of values of ν. (c) The time series $r_+(t)$ (thick line) and $r_-(t)$ (thin line) corresponding to case (b) with $\mu = 0.02$. (d) The quantity $[r_+(t) + r_-(t)\cos(\omega_2 t)]\sin(\omega_1 t)$ corresponding to (c) when $\omega_1 = 20.0$ and $\omega_2 = 0.8$ for comparison with Fig. 6. Note the exponential growth during the chevron phase, followed by an overshoot when the blinking instability sets in, and the ringing down during the subsequent collapse phase.

that $a_+<0$ and the saddle-node bifurcation is therefore absent. As a result the chevrons are initially stable, and the bifurcation to the blinking states occurs for $\mu>0$. In contrast, when $\nu<a_+b_-/2=1$ the first stable state encountered as μ increases is a periodic state $[r_+(t),r_-(t)]$ corresponding to the three-frequency repeated transient state with the frequencies ω_1 and ω_2 filtered out [Fig. 25(b)]. This state appears in a global bifurcation at $\mu=\mu^*<0$, at which $\omega_3=0$. Figure 25(c) shows the time series corresponding to this state when $\mu=0.02$, $\nu=0.15$, $a_+=2.0$, $a_-=-0.2$, and $b_-=1.0$. For these parameter values $\mu^*\approx 0$ [open circles in Fig. 25(b)], and Fig. 24 shows that this situation persists for a large range of values of ν. In this case the chevron state regrows from a very small amplitude, and the resulting oscillation resembles closely the state shown in Fig. 6. In particular, there is almost no hysteresis between this state and the conduction state, and the system behaves as if the primary instability at $\mu=0$ were directly responsible for generating repeated transients. Observe that during the growth phase of the variable r_+ the variable r_- vanishes, indicating that the growing state is a pure chevron; r_- becomes nonzero only during the collapse phase, indicating that the collapse is triggered by a symmetry-breaking instability of the growing even chevron. The amplitude and the period $2\pi/\omega_3$ of the limit cycle in Fig. 25(c) decrease with increasing μ, with the oscillations disappearing at H_3. As already mentioned we interpret this transition as the transition from the repeated transient state to the (symmetric) periodic blinking state with increasing Rayleigh number seen in Fig. 8. For the model parameters (and in contrast to the corresponding transition in water-ethanol mixtures[8]) this transition is *supercritical*, indicating absence of hysteresis, as in the figure.

Within the model the repeated transient state $[r_+(t),r_-(t)]$ has all the properties of this state observed in the simulations, except for the (apparent) absence of oscillations during the collapse phase. In fact, if the frequencies ω_1 and ω_2 are restored, and the pointwise quantity $[r_+(t)+r_-(t)\cos\omega_2 t]\sin\omega_1 t$, cf. Eq. (13), plotted instead of $r_+(t)$ or $r_-(t)$, these oscillations are present [Fig. 25(d)], and their amplitude depends on the chevron amplitude r_+ in the manner observed in the simulations. In fact, the time series shown in Fig. 25(d) bears a number of qualitative features, including the pointed overshoot at maximum as the mode r_- begins to grow and the "ringing down" due to the fact that the variable r_+ decays more rapidly than r_-, that are documented in experiments as well [Fig. 6(a) of Ref. 4].

Despite its remarkable simplicity the model [(14) – (15)] captures completely the two scenarios for generating blinking states identified in the simulations of both ^{3}He–^{4}He and water-ethanol mixtures, and the origin and properties of the repeated transients. Extensions of the model[8] indicate the possibility that repeated transients may, under appropriate circumstances, be chaotic. In Fig. 26 we show an example of such a chaotic repeated transient state. We believe that this state is associated with the global bifurcation in which the repeated transients first appear, cf. Fig. 25(b). As already noted the frequency ω_3 decreases to zero as $\mu\downarrow\mu^*<0$, i.e., as $\epsilon\downarrow\epsilon^*<0$ in the partial differential equations. As this occurs the three-frequency states approach simultaneously the

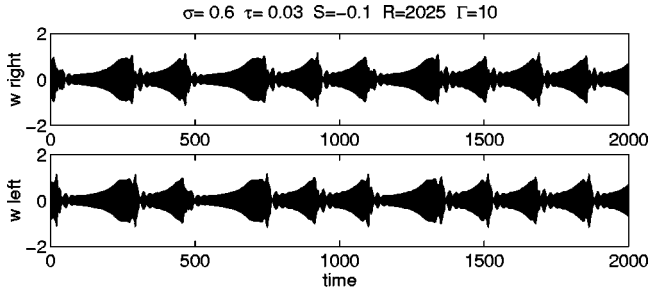

FIG. 26. A chaotic repeated transient in a ^{3}He–^{4}He mixture with stress-free and fixed temperature boundary conditions at $x=0,\Gamma$ and $R=2025$, $S=-0.1$, $\sigma=0.6$, $\tau=0.03$, and $\Gamma=10$.

unstable large and small amplitude chevron states, hereafter A and B, respectively (see Fig. 25). The character of the repeated transient when $\epsilon\approx\epsilon^*$ is determined by the leading eigenvalues of A and B in the $(r_+,0)$ direction, hereafter $-\lambda_A<0$ and $\lambda_B>0$, and the leading eigenvalues in the $(0,r_-)$ direction. If the latter are real, $\alpha_A>0$ and $-\alpha_B<0$, say, and $\rho\equiv\alpha_B\lambda_A/\alpha_A\lambda_B>1$, the repeated transients will remain periodic and stable all the way to ϵ^*, where the period T_3 diverges and the global bifurcation takes place.[8] In contrast, when $0<\rho<1$, the periodic oscillations necessarily lose stability before the global bifurcation at ϵ^*. Similar results obtain in the case where the leading stable symmetry-breaking eigenvalue at B is complex, viz., $-\alpha_B+i\omega_B$, $\alpha_B>0$, as suggested by the simulations. In this case stable periodic oscillations will persist down to ϵ^* if $\rho>1$, but if $0<\rho<1$ complex dynamics of Shil'nikov type will be present. In fact, the leading unstable eigenvalues α_A and λ_B are also expected to be complex, since in the partial differential equations the bifurcations at H_1 and H_2 are both Hopf bifurcations.

When λ_B is real a trajectory escaping from B describes an exponentially growing chevron state. This growth phase, including the states A and B, is clearly visible in the time series in Fig. 6. When the growing chevron reaches the vicinity of A it becomes unstable to symmetry-breaking oscillations which take it back near B. This is the collapse phase of the repeated transient state [compare Fig. 25(d) with Fig. 6]. The frequency of the decaying oscillations observed in the time series in Figs. 25(d) is given by ω_B. This frequency will in general be of the same order as the blinking frequency associated with the branch of blinking states when these bifurcate from the small amplitude chevron B, but quite different from (and in general larger than) the blinking frequency of the *stable* blinking states beyond H_3, cf. Ref. 4. This observation explains the coincidence of the period of the blinking states and of the oscillations during the collapse phase of the repeated transient noted by Kolodner. Note also that since α_B decreases as ϵ decreases (it passes through zero at H_2, i.e., at $\epsilon=\epsilon_2$) the collapse becomes slower and slower, cf. Fig. 6, although the collapse rate is still finite when the three-frequency states disappear in the global bifurcation at ϵ^* (since $\epsilon_2<\epsilon^*<0$) and the system makes a hysteretic transition back to the conduction state. The fact that α_B decreases with ϵ makes it likely that the Shil'nikov condition $0<\rho<1$ holds at ϵ^*, resulting in *chaotic* repeated transients prior to their disappearance. However, despite this suggestion we

have only succeeded in locating such chaotic repeated transients with *stress-free* boundary conditions (Fig. 26).

V. DISCUSSION

In this article we have described the results of direct numerical simulations of oscillatory convection in binary mixtures in two-dimensional moderately large domains with experimentally relevant boundary conditions, exploring in detail the parameter values characteristic of ^{3}He–^{4}He mixtures. We have chosen ^{3}He–^{4}He parameters partly because of a number of experiments on this system in the 1980s (Refs. 1 and 10–12) and partly to make predictions for future experiments now that flow visualization at cryogenic temperatures has become possible.[13] We have also used smaller domains in order to reduce the length of the immensely long transients encountered in our simulations of water-ethanol mixtures.[8] As a result we have been able to explore a larger range of values of the Rayleigh number, reaching values at which the low-dimensional description of this system valid near threshold begins to breakdown. We have argued that this transition occurs once $|\epsilon| \sim \Gamma^{-2}$ and provided numerical evidence in support of this claim. Among the new phenomena that occur once $|\epsilon| \gtrsim \Gamma^{-2}$ are the *fish states* originally observed by Kolodner, Surko, and Williams in water-ethanol mixtures[2] and various types of dynamically localized traveling-wave states also seen in experiments.[26–28]

For $|\epsilon| \lesssim \Gamma^{-2}$ the dynamics of the system can be understood in detail using a low-dimensional description based on the interaction of adjacent pure parity chevron states whose structure is known from linear theory, as summarized in Sec. IV. These states interact strongly at small amplitude in the vicinity of mode interaction points, i.e., specific values of the aspect ratio Γ at which both modes bifurcate from the conduction state simultaneously.[7] These mode interaction points correspond to a double Hopf bifurcation with generically nonresonant frequencies. Unfolding of the normal form for this bifurcation to take into account the splitting of the mode interaction leads to a pair of simple equations for the amplitudes of the two competing modes. It is a remarkable fact that these equations describe all the qualitative behavior of the system for $|\epsilon| \lesssim \Gamma^{-2}$, including the blinking and repeated transient states and the transitions between them, provided only that one takes into account the fact that the primary instability to the chevron state is generally subcritical. In particular, the model constructed in Sec. IV shows that the repeated transients are a three-frequency state, and explains why it is so often the first nontrivial state observed in the simulations once the conduction state loses stability, and why it often appears without observable hysteresis. The model also shows that with increasing Rayleigh number the lowest of the three frequencies in the repeated transient state disappears in a tertiary Hopf bifurcation, leaving behind a stable large amplitude blinking state. In the model, as in the simulations, this bifurcation is supercritical and hence is nonhysteretic. In contrast, the corresponding bifurcation in water-ethanol mixtures was found to be always subcritical and hence hysteretic.[8] Finally, the model also suggests the possibility of chaotic repeated transients, and we were able to find such states in ^{3}He–^{4}He mixtures, although only with stress-free boundary conditions. In principle the coefficients in the model can be calculated from Eqs. (1)–(6) in terms of the physical parameters of the system. This is a major undertaking, however, and is beyond the scope of this paper. Consequently our interpretation of the simulations remains qualitative.

When $|S|$ is sufficiently small the dynamics remains low dimensional through the transition from the blinking states to steady convection. The nature of this transition can be understood on the basis of existing theory for the Hopf bifurcation with broken $O(2)$ symmetry.[5,16,19,20] In this theory the loss of translation invariance due to the presence of sidewalls is treated as a perturbation of the unbounded system with periodic boundary conditions. This approach is appropriate at larger ϵ since the effect of sidewalls *weakens* with increasing ϵ. With periodic boundary conditions Eqs. (1)–(6) possess $O(2)$ symmetry, and both standing waves (SW) and traveling waves (TW) bifurcate from the conduction state *simultaneously*. Weakly nonlinear theory shows that for typical parameter values both bifurcate subcritically, with the TW more subcritical than the SW.[16] The presence of distant boundaries splits apart this multiple bifurcation but does not change the direction of the branching. Odd and even SW, to be identified with the odd- and even-parity chevrons, are now the only states that bifurcate from the conduction state; the analog of the traveling waves bifurcates from one or other chevron branch in a secondary steady-state bifurcation, and takes the form of a single frequency state that is neither odd nor even under left-right reflection. These states, hereafter TW′, resemble asymmetric chevrons near the secondary bifurcation, but pure traveling waves at large enough amplitude.[5,19,20] This bifurcation is present even when the chevrons are subcritical, and in smaller domains will occur beyond the saddle-node bifurcation that stabilizes them. Since the TW are generally more subcritical than the SWs it is likely that this steady-state bifurcation will remain subcritical; the resulting TW′ will therefore remain unstable. However, as shown elsewhere,[15,19,20] for appropriate aspect ratios this steady bifurcation may be preceded by a Hopf bifurcation producing blinking states, which in turn terminate in a global (heteroclinic) bifurcation connecting the two symmetry-related TW′. The behavior of the blinking frequency ω_2 provides the signature of this bifurcation: as this bifurcation is approached ω_2 vanishes *logarithmically*, cf. Eq. (9), while ω_1 remains finite. Since the TW′ are unstable the solution then jumps to the only other stable state available, steady overturning convection. This scenario is entirely consistent with the results obtained numerically for $S = -0.001$ in Figs. 1–4. A similar transition has also been seen in experiments on water-ethanol mixtures.[2] Note that this scenario applies for relatively small values of $|S|$, for which the Takens–Bogdanov (TB) point $S = S_{\mathrm{TB}}$ is not far, and a low-dimensional description is therefore appropriate.

Once $|\epsilon| \gtrsim \Gamma^{-2}$ the above scenario may continue to hold, but only if the separation ratio S is tuned at the same time. Our simulations reveal that for generic $O(1)$ values of S the behavior becomes dramatically different. This regime is characterized by the so-called fish state, first observed in

water-ethanol mixtures,[2] and it is the vanishing of the chevron frequency ω_1, instead of ω_2, that now appears to be responsible for the cessation of the blinking state as ϵ increases. We surmise that, in this regime, as ϵ increases the amplitude of the chevron becomes large enough that nonlinear corrections reduce the frequency ω_1 locally to zero. In this region the state ceases to propagate and resembles (locally) steady overturning convection. Flows of this type homogenize the mixture, and permit the formation of an inclusion of steady overturning convection of substantially larger amplitude, cf. Fig. 5. Such inclusions are not stable, however, and the steady state expands, invading the rest of the domain, and replacing the time-dependent state by a time-independent localized or extended state. A transition of this type corresponds (locally) to a jump from an unstable *steady* convection state to a larger amplitude stable steady state, as seen in Fig. 5. However, from a global perspective the details of this transition remain unclear.

The fish state (Fig. 10) is the first manifestation of the transition to a large number of degrees of freedom ($\epsilon \gtrsim \Gamma^{-2}$), the fish phase corresponding to temporary but dynamic confinement of the traveling-wave state. The hallmark of dynamic confinement is the essentially complete absence of counterpropagating waves. This is seen not only in the wall-attached state in Fig. 18 but also in the space-time plots in Figs. 11 and 17. In a dynamically confined state the finite amplitude traveling waves are separated from the convection-free region (i.e., a region of exponentially small waves) by a sharp front of $O(\epsilon^{-1/2})$ width; the transition between this regime and the low-dimensional regime dominated by chevron-like states occurs when the width of the front becomes comparable to the size of the domain, i.e., $|\epsilon|\Gamma^2 \sim 1$. The latter regime is dominated by sidewalls and any localization can be at most kinematic.[20] In the kinematic regime the amplitude of the counterpropagating wave is never zero, and a kinematically localized state near the left sidewall always shows a small amplitude right-traveling wave near the right sidewall, i.e., such a localized state is nothing but a strongly asymmetric chevron.[20,40] Our simulations are broadly consistent with these ideas.

For example, in Fig. 10 $\Gamma=10$ and $\epsilon=2.35\times10^{-2}$ so that $|\epsilon|\Gamma^2=2.35$, while in Ref. 2, where the fish state was first observed, $\Gamma=16.75$ and $\epsilon=0.0103$, giving $|\epsilon|\Gamma^2=2.89$. Both of these examples represent marginal cases just outside of the low-dimensional description. The experiment in Ref. 21 on water-ethanol mixtures is further in the high-dimensional regime. Here $\Gamma=40.6$ and $\epsilon=0.0094$, giving $|\epsilon|\Gamma^2=15.49$. Indeed the authors argue[21] that for sufficiently large ϵ the dynamics of the system resembles more and more the collapse events described by a single subcritical Ginzburg–Landau equation on an *unbounded* domain. In fact, the experiments of Ref. 21 suggest that this is so once $|\epsilon|\Gamma^2 \gtrsim 10$, while those of Ref. 23, performed for slightly larger $|S|$ and subcritical values of ϵ, suggest the requirement $|\epsilon|\Gamma^2 \gtrsim 5$. Our simulations indicate that the location of the transition to high-dimensional behavior depends quite sensitively on the value of $|S|$, although in all cases $|\epsilon|\Gamma^2$ remains of order one. For example, our results for $S=-0.021$ yield $|\epsilon|\Gamma^2 \sim 0.3$; for $S=-0.5$ the transition to the fish state and subsequent transitions probably all take place at negative values of ϵ, not considered here.

The temporarily localized traveling-wave states shown in Fig. 12 resemble in structure the so-called localized traveling-wave (LTW) states found in Ref. 41 in extensive simulations of binary mixtures with laterally periodic boundary conditions and water-ethanol parameters. However, in our case these states have a lower frequency than the corresponding chevrons, in contrast to the LTW of Ref. 41 which have a substantially higher frequency than the spatially uniform TW at the same parameters.[41,42] Of course, our localized states are unstable and may not be related to those of Ref. 41 which are unaffected by lateral walls. In addition our states are present at substantially positive values of ϵ. It is noteworthy that with our boundary conditions we have been unable to find stable finite amplitude traveling waves that fill the entire domain. All our solutions always eventually break up into the type of states described in Sec. III. Although there is no evidence that ^{3}He–^{4}He mixtures support spatially homogeneous traveling waves (modulo end effects) waves of this type have been observed in rectangular containers filled with water-alcohol mixtures. This unexpected observation may be related to the fact that traveling waves in ^{3}He–^{4}He mixtures are typically more subcritical than in water-ethanol mixtures,[16] while the opposite is the case for standing waves (i.e., chevrons, in finite domains).

ACKNOWLEDGMENTS

This work was supported by an EPSRC Grant No. GR/R52879/01 and the National Science Foundation under Grant No. DMS-0072444. Computer time was provided by CEPBA. We thank I. Mercader and M. Net for assistance.

[1] T. S. Sullivan and G. Ahlers, "Nonperiodic time dependence at the onset of convection in a binary liquid mixture," Phys. Rev. A **38**, 3143 (1988).
[2] P. Kolodner, C. M. Surko, and H. Williams, "Dynamics of traveling waves near the onset of convection in binary fluid mixtures," Physica D **37**, 319 (1989).
[3] V. Steinberg, J. Fineberg, E. Moses, and I. Rehberg, "Pattern selection and transition to turbulence in propagating waves," Physica D **37**, 359 (1989).
[4] P. Kolodner, "Repeated transients of weakly nonlinear traveling-wave convection," Phys. Rev. E **47**, 1038 (1993).
[5] G. Dangelmayr and E. Knobloch, "Hopf bifurcation with broken circular symmetry," Nonlinearity **4**, 399 (1991).
[6] A. S. Landsberg and E. Knobloch, "Oscillatory bifurcation with broken translation symmetry," Phys. Rev. E **53**, 3579 (1996).
[7] O. Batiste, I. Mercader, M. Net, and E. Knobloch, "Onset of oscillatory binary fluid convection in finite containers," Phys. Rev. E **59**, 6730 (1999).
[8] O. Batiste, E. Knobloch, I. Mercader, and M. Net, "Simulations of oscillatory binary fluid convection in large aspect ratio containers," Phys. Rev. E **65**, 016303 (2001).
[9] D. R. Caldwell, "Experimental studies on the onset of thermohaline convection," J. Fluid Mech. **64**, 347 (1974).
[10] G. Ahlers and I. Rehberg, "Convection in a binary mixture heated from below," Phys. Rev. Lett. **56**, 1373 (1986).
[11] T. S. Sullivan and G. Ahlers, "Hopf bifurcation to convection near the codimension-two point in a ^{3}He–^{4}He mixture," Phys. Rev. Lett. **61**, 78 (1988).
[12] T. J. Bloodworth, M. R. Ardron, J. K. Bhattacharjee, P. G. J. Lucas, and N. D. Stein, "Convection in ^{3}He–^{4}He mixtures with large negative separation ratios," Nonlinearity **3**, 981 (1990).
[13] A. L. Woodcraft, P. G. J. Lucas, R. G. Matley, and W. Y. T. Wong, "Visualisation of convective flow patterns in liquid helium," J. Low Temp. Phys. **114**, 109 (1999).

[14]O. Batiste and E. Knobloch, in *Perspectives and Problems in Nonlinear Science*, edited by E. Kaplan, J. Marsden, and K. Sreenivasan (Springer, Berlin, 2003), pp. 91–144.
[15]E. Knobloch, M. R. E. Proctor, and N. O. Weiss, in *Turbulence in Fluid Flows: A Dynamical Systems Approach*, IMA Volumes in Mathematics and its Applications Vol. 55, edited by G. R. Sell, C. Foias, and R. Temam (Springer, New York, 1993), pp. 59–72.
[16]T. Clune and E. Knobloch, "Mean flow suppression by endwalls in oscillatory binary fluid convection," Physica D **61**, 106 (1992).
[17]S. Hugues and A. Randriamampianina, "An improved projection scheme applied to pseudospectral methods for the incompressible Navier-Stokes equations," Int. J. Numer. Methods Fluids **28**, 501 (1998).
[18]S. Zhao and M. J. Yedlin, "A new iterative Chebyshev spectral method for solving the elliptic equation $\nabla\cdot(\sigma\nabla u)=f$," J. Comput. Phys. **113**, 215 (1994).
[19]G. Dangelmayr and E. Knobloch, in *The Physics of Structure Formation: Theory and Simulation*, edited by W. Güttinger and G. Dangelmayr (Springer, Berlin, 1987), pp. 387–393.
[20]G. Dangelmayr, E. Knobloch, and M. Wegelin, "Travelling wave convection in finite containers," Europhys. Lett. **16**, 723 (1991).
[21]E. Kaplan, E. Kuznetsov, and V. Steinberg, "Burst and collapse in traveling-wave convection of a binary fluid," Phys. Rev. E **50**, 3712 (1994).
[22]P. Kolodner, "Neutrally stable fronts of slow convective traveling waves," Phys. Rev. A **42**, 2475 (1990).
[23]J. J. Niemela, G. Ahlers, and D. S. Cannell, "Localized traveling-wave states in binary-fluid convection," Phys. Rev. Lett. **64**, 1365 (1990).
[24]A. E. Deane, E. Knobloch, and J. Toomre, "Travelling waves in large-aspect-ratio thermosolutal convection," Phys. Rev. A **37**, 1817 (1988).
[25]C. Martel and J. M. Vega, "Dynamics of a hyperbolic system that applies at the onset of the oscillatory instability," Nonlinearity **11**, 105 (1998).
[26]R. Heinrichs, G. Ahlers, and D. S. Cannell, "Traveling waves and spatial variation in the convection of a binary mixture," Phys. Rev. A **35**, 2761 (1987).
[27]E. Moses, J. Fineberg, and V. Steinberg, "Multistability and confined traveling-wave patterns in a convecting binary mixture," Phys. Rev. A **35**, 2757 (1987).
[28]P. Kolodner, "Stable and unstable pulses of traveling-wave convection," Phys. Rev. A **43**, 2827 (1991).
[29]H. Yahata, "Travelling convection rolls in a binary fluid mixture," Prog. Theor. Phys. **85**, 933 (1991).
[30]L. Ning, Y. Harada, and H. Yahata, "Modulated traveling waves in binary fluid convection in an intermediate-aspect-ratio rectangular cell," Prog. Theor. Phys. **97**, 831 (1997).
[31]M. C. Cross, "Traveling and standing waves in binary-fluid convection in finite geometries," Phys. Rev. Lett. **57**, 2935 (1986).
[32]M. C. Cross, "Structure of nonlinear traveling-wave states in finite geometries," Phys. Rev. A **38**, 3593 (1988).
[33]S. Tobias, M. R. E. Proctor, and E. Knobloch, "Convective and absolute instabilities of fluid flows in finite geometry," Physica D **113**, 43 (1998).
[34]H. Riecke, "Self-trapping of traveling-wave pulses in binary mixture convection," Phys. Rev. Lett. **68**, 301 (1992).
[35]H. Riecke and W.-J. Rappel, "Coexisting pulses in a model for binary-mixture convection," Phys. Rev. Lett. **75**, 4035 (1995).
[36]S. Blanchflower, "Magnetohydrodynamic convectons," Phys. Lett. A **261**, 74 (1999).
[37]P. Kolodner, "Coexisting traveling waves and steady rolls in binary-fluid convection," Phys. Rev. E **48**, R665 (1993).
[38]J. Guckenheimer, in *Dynamical Systems and Turbulence*, Lecture Notes in Mathematics Vol. 898, edited by D. A. Rand and L. S. Young (Springer, New York, 1981), pp. 99–142.
[39]E. Knobloch and D. R. Moore, "A minimal model of binary fluid convection," Phys. Rev. A **42**, 4693 (1990).
[40]V. Croquette and H. Williams, "Nonlinear competition between waves on convection rolls," Phys. Rev. A **39**, 2765 (1989).
[41]W. Barten, M. Lücke, M. Kamps, and R. Schmitz, "Convection in binary fluid mixtures. II. Localized traveling waves," Phys. Rev. E **51**, 5662 (1995).
[42]D. Jung and M. Lücke, "Localized waves without the existence of extended waves: oscillatory convection of binary mixtures with strong Soret effect," Phys. Rev. Lett. **89**, 054502 (2002).